

New insights into the production of sustainable synthetic aggregates and their microstructural evaluation

R. Vignesh, A. Abdul-Rahim✉

Department of Structural and Geotechnical Engineering, School of Civil Engineering,
Vellore Institute of Technology, (Vellore, India)
✉: abdulrahim.a@vit.ac.in

Received 10 November 2022
Accepted 19 April 2023
Available on line 28 July 2023

ABSTRACT: In this study, a novel technique for producing synthetic aggregates using industrial by-products was experimentally investigated. Taguchi method is used to identify the optimum mix design proportion to develop durable synthetic aggregates. For this, different combinations of quaternary binders including ordinary Portland cement, ground granulated blast furnace slag, metakaolin, and lime powder was used. The obtained results revealed that the synthetic aggregates prepared with optimized mortar mix enhanced the compressive strength by 5.9%. Then the performance of synthetic aggregates was evaluated based on their mechanical and durability properties. Microstructural properties of the produced aggregates were examined. The results showed that optimum mix is highly effective than control mix. The manufactured synthetic aggregates are in accordance with the ASTM C 330 standard requirements. Therefore, our study contributes to the advancement in the sustainability by developing a method for producing synthetic aggregates from industrial byproducts.

KEY WORDS: Synthetic aggregates; Taguchi method; Blast furnace slag; Natural aggregates; Quaternary binders; Sustainability.

Citation/Citar como: Vignesh, R.; Abdul Rahim, A. (2023) New insights into the production of sustainable synthetic aggregates and their microstructural evaluation. *Mater. Construcc.* 73 [351], e324. <https://doi.org/10.3989/mc.2023.328722>.

RESUMEN: *Nuevos conocimientos sobre la producción de áridos sintéticos sostenibles y su evaluación microestructural.* En este estudio se investigó experimentalmente una nueva técnica para producir áridos sintéticos utilizando subproductos industriales. El método de Taguchi se utiliza para identificar la proporción de diseño de mezcla óptima para desarrollar áridos sintéticos duraderos. Para ello, se utilizaron diferentes combinaciones de aglomerantes cuaternarios que incluían cemento Portland ordinario, escoria de alto horno granulada molida, metacaolín y polvo de cal. Los resultados obtenidos revelaron que los áridos sintéticos preparados con mezcla de mortero optimizada mejoraron la resistencia a la compresión en un 5,9%. Luego se evaluó el desempeño de los áridos sintéticos en base a sus propiedades mecánicas y de durabilidad. Se examinaron las propiedades microestructurales de los áridos producidos. Los resultados mostraron que la mezcla óptima es más efectiva que la mezcla de control. Los áridos sintéticos fabricados cumplen con los requisitos de la norma ASTM C 330. Por tanto, nuestro estudio contribuye al avance de la sostenibilidad mediante el desarrollo de un método para producir áridos sintéticos a partir de subproductos industriales.

PALABRAS CLAVE: Áridos sintéticos; Método Taguchi; Escorias de alto horno; Áridos naturales; Conglomerantes cuaternarios; Sostenibilidad.

Copyright: ©2023 CSIC. This is an open-access article distributed under the terms of the Creative Commons Attribution 4.0 International (CC BY 4.0) License.

1. INTRODUCTION

Demand for innovative construction materials is high due to expeditious development in population and rapid construction activities to meet the requirement of global infrastructure development. Around the world, the natural resources are getting depleted at a very faster rate. Rapid industrialization generates enormous quantities of industrial by-products that are not feasible for society and difficult to handle. Consuming the industrial by-products as building materials is a safe and eco-friendly method of disposing waste and preserves the natural resources for the forthcoming generation (1). In the past few decades, concrete has been the most popular building material in the world due to its numerous benefits. In addition, it is a considerably less expensive material and holds a longer life with less maintenance.

Aggregates play an important role in giving concrete its structure, comprising about 60–80% of the volume of concrete and having a significant effect on the properties of the concrete (2). Continuous aggregate extraction must deplete natural resources. In addition, quarrying and the process of natural aggregates directly contribute to the generation of dust, noise, and carbon dioxide, all of which have an adverse effect on the environment. Therefore, more attention was given to producing artificial aggregates from various industrial and municipal wastes to produce durable concrete aggregates (3). From the previous literature, the synthetic aggregates have enormous applications, including the production of prefabricated structural elements, structural concrete, thermal protection, sound insulation, landscaping, hydroponics, and soil investigation operations (4). Therefore, establishing a new source of coarse aggregates is a critical concern for modern civilization (5). Artificial aggregates are manufactured using one of three methods: sintering, autoclaving, or cold-bonding pelletization (6). In most cases, artificial aggregates are produced using a high temperature sintering process. Lightweight expanded clay aggregate (LECA) is one kind of synthetic aggregate primarily made at particularly high calcination temperatures from 900°C to 1200°C (7). However, sintering is a more energy-consuming method. In addition, this sintering process generates harmful gases and pollutants while producing artificial aggregates (8). Cold-bonding is a process that requires the curing of aggregates at ambient temperature or in a steam-filled confined area until the required strength is achieved. On the other hand, the cold bonding method requires cementitious materials and takes more time (28 days) to produce aggregates with the desired properties of strength (9). Because of its lower energy requirement, this cold-bonding method is more economical than the sintering method, even though it occupies more time to achieve its mechanical property.

Naturally available lightweight aggregates (LWA) including basalt, pumice, and diatomite are formed from volcanic rocks. However, LWAs are artificially manufactured, with the main process involving mixing raw materials, agglomeration, and particle binding, followed by post-processing (curing) owing to the increasing need for lightweight concrete (10). The manufactured synthetic lightweight aggregates contain various industrial by-products including furnace slag, sedimented bottom ash, and rubber-based waste (11). Therefore, the best approach to conserve the environment and natural resources is to replace natural aggregates in structural concrete with synthetic aggregates produced from industrial by-products or hazardous wastes (12). According to previous literature, natural coarse aggregate with a greater unit weight benefits lightweight synthetic aggregate production. The most important quality of synthetic aggregates is bulk density. The lightweight aggregates mostly produce less dense microstructure and absorb more water, decreasing the mechanical strength (13). However, continuous efforts and dedication to develop new hybrid synthetic aggregates by utilizing different binders are gaining popularity because carbon dioxide emissions from the cement manufacturing process caused a threat to the environment (14).

Developing an economically viable binder from sources of industrial by-products remains the major challenge in meeting the cement production deficiency. So, to overcome this problem, generated industrial wastes such as fly ash, blast furnace slag, silica fume and natural pozzolanic materials such as limestone powder, calcined clay were also utilized (15). Especially, GGBFS has been extensively investigated and utilized as supplementary cementitious material for a variety of applications. The prior research suggested that a higher amount of C-S-H gel development was observed when GGBFS was utilized as an alternative to OPC. Metakaolin is one of the known supplementary cementitious materials made by calcining a natural clay product kaolin at a temperature ranging between 500 and 800 °C (16). Metakaolin improves the mechanical properties of Ordinary Portland cement-metakaolin binder systems, acquires a good packing effect and improves the reaction between these pozzolanas (16). Along fly ash and GGBFS, the slaked lime at a maximum of 5% of a binder improves the mechanical qualities of geopolymer concrete (17). Thus, the reuse of industrial wastes and the use of recycled materials in construction projects have become widespread globally in the last few decades (18). From the literature, the Taguchi technique was utilized as an effective tool to produce quality products with fewer experiments, thereby saving time and expenditure (19). The Taguchi approach makes it simple to design an experimental study by determining the optimal operating settings for the parameters that affect the

outcome (20). Previous studies have reported that the Taguchi approach effectively optimized different parameters (21-24). This paper aims to conduct an experimental study on the manufacturing and examination of synthetic aggregates.

When several factors have to be evaluated, the Taguchi approach is a systematic method for discovering the “optimal” set of inputs in order to generate a product with optimum features. The Taguchi technique use orthogonal arrays from the theory of design of experiments to examine a lot of variables with a minimum set of experiments. Due to the rapid transformation of global infrastructure development, aggregate usage is growing tremendously. However, the available natural resources are extremely limited, and mining has major ecological effects. Therefore, it is required to develop alternative aggregates using available indigenous materials. These artificial aggregates can substitute natural aggregates in the construction industry. The purpose of this study is to develop synthetic aggregates utilizing the industrial byproducts as binders. This article is structured as follows: (i) the production method of synthetic aggregates by using the design of experiments; (ii) to utilize industrial by-products as source materials to produce synthetic aggregates and their influence on the properties of synthetic aggregates (iii) to assess the physical, mechanical, and durability properties of produced synthetic aggregates (iv) to examine the microstructural properties of synthetic aggregates.

2. EXPERIMENTAL PROGRAMME

2.1. Materials

Ordinary Portland cement (OPC) of grade 53 was purchased from Zuari Cement located in Vellore, India and used as a binder following ASTM C150 (25). According to Table 1, the specific gravity and specific surface area of cement are 3.15 g/cc and 3194 cm²/g, respectively. Ground granulated blast furnace slag (GGBFS) was obtained from the steel production industry (Salem, India) as per ASTM C989 (26). The quantity of oxides and some other chemical components present in the binders are shown in Table 2. Metakaolin (MK) was purchased from Jeetmull Jaichandlall Madras Pvt. Ltd., Chennai, India., which class N

was as per ASTM C618 (27). Hydrated lime powder (LP) is a dry powder manufactured from limestone. This lime stone calcined under high temperature. Then the calcined lime stone is slaked with water. To convert oxides into hydroxides, quicklime (CaO) is hydrated with water. This hydrated lime is chemically known as calcium hydroxide (Ca (OH)₂). In this study, hydrated lime powder with a particle size of 3.39 μm (as depicted in Table 1) was used as filler material to fill the pores present in the synthetic aggregates. The incorporation of lime into mortars enhances workability and reduces porosity.

A quaternary blended binder system such as cement, GGBFS, metakaolin, and lime powder is utilized to manufacture synthetic aggregates. Figure 1 depicts the distribution of particles size of the binders used in this study. Riverbed sand collected from Vellore with a specific gravity of 2.66 and fineness modulus of 2.72 was utilized as fine aggregates. These fine aggregates had a loose bulk density of 1468.86 kg/m³. The water absorption was determined to be very less as 1.04%. A high-range water reducer (Polycarboxylic ether based) named Master Glenium SKY 8108 was used in this study to minimize the water required and to improve the workability significantly. As indicated in Figure 2, this investigation uses polypropylene fibers as fiber reinforcement. The fibers have an L/D aspect ratio of 300 and a tensile strength of 450 MPa in the form of continuous of 12 mm length monofilaments with a 40μm diameter of circular cross-section. Large peaks of calcium carbonate (calcite) are visible in the diffractograms

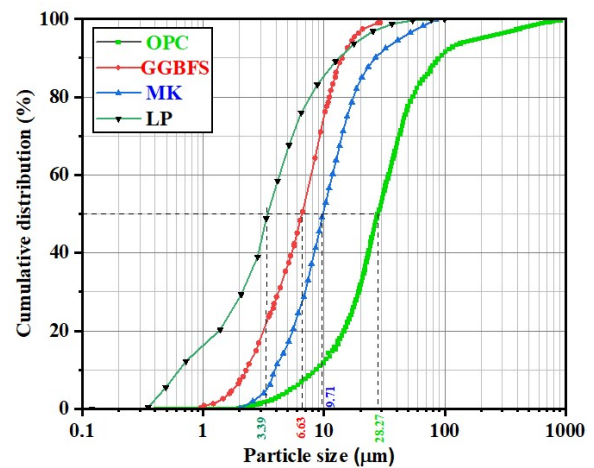


FIGURE 1. Particle size distribution curve of raw binders.

TABLE 1. Physical properties of raw binders.

Raw binders	Specific gravity (g/cc)	Specific surface area (cm ² /g)	Median particle size D ₅₀ (μm)
OPC	3.15	3194	28.27
GGBFS	2.86	5128	6.63
MK	2.62	13286	9.71
LP	2.34	8764	3.39

TABLE 2. Composition of the oxides present in binders.

Binders	Oxides (%)										
	SiO ₂	TiO ₂	Al ₂ O ₃	MnO	Fe ₂ O ₃	CaO	MgO	Na ₂ O	K ₂ O	P ₂ O ₅	SO ₃
OPC	18.6	0.36	4.45	0.07	4.45	63.9	1.1	0.19	0.54	0.35	4.81
GGBFS	36.7	0.92	16.6	1.26	0.45	35.1	6.11	0.2	0.53	0.06	1.27
MK	53	1.49	43.5	-	0.91	0.31	-	0.17	0.16	0.11	0.1
LP	1.27	-	0.17	-	0.09	94.4	2.48	-	-	-	0.4

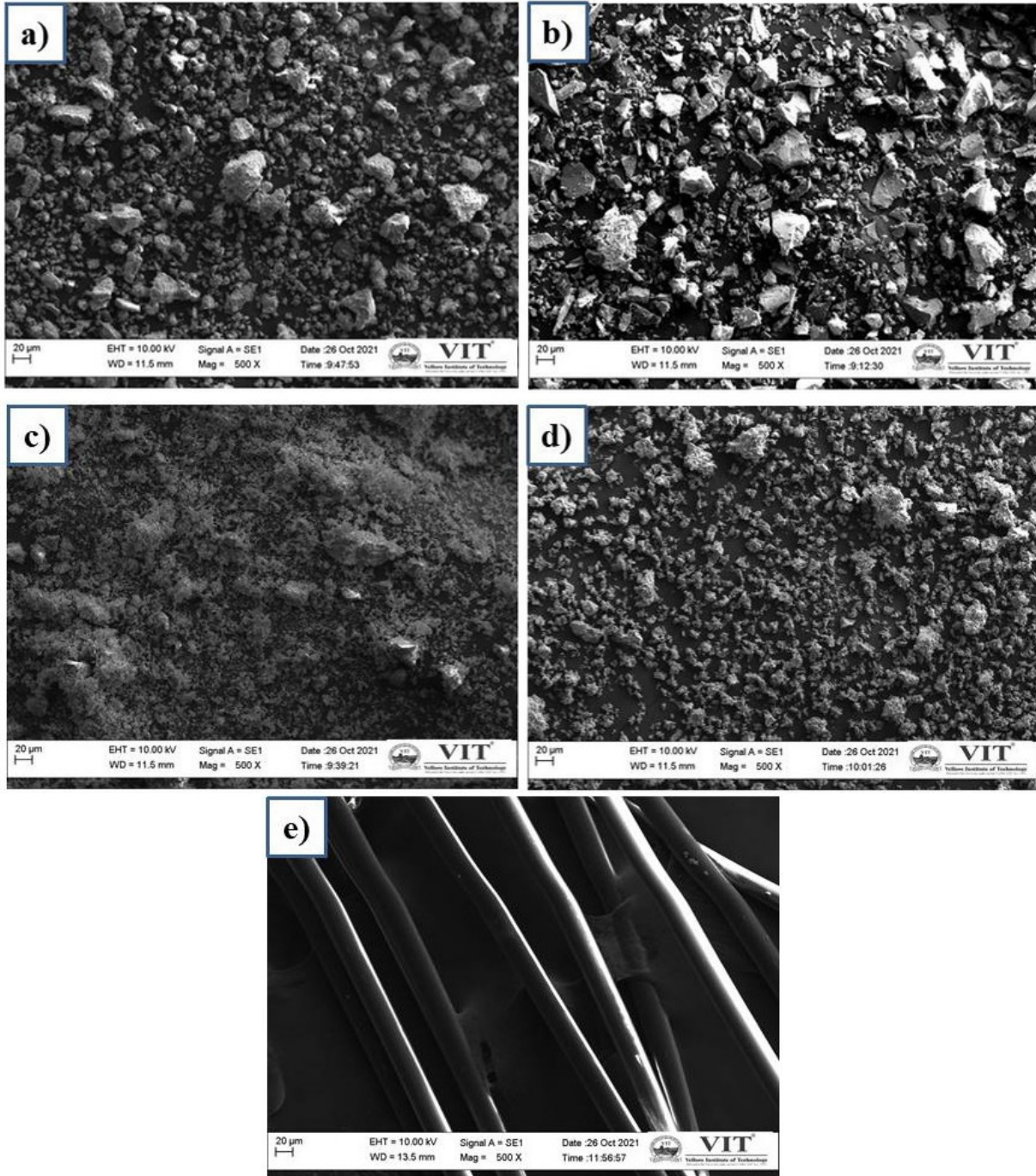


FIGURE 2. Morphological view of (a) OPC (b) GGBFS (c) MK and (d) LP (e) PPF.

for powdered limestone. Quartz peaks are observed in metakaolin diffractograms. Additionally, several peaks of kaolinite are identified. Alite and Belite were identified as the predominant phases of ordinary Portland cement, as shown in Figure 3.

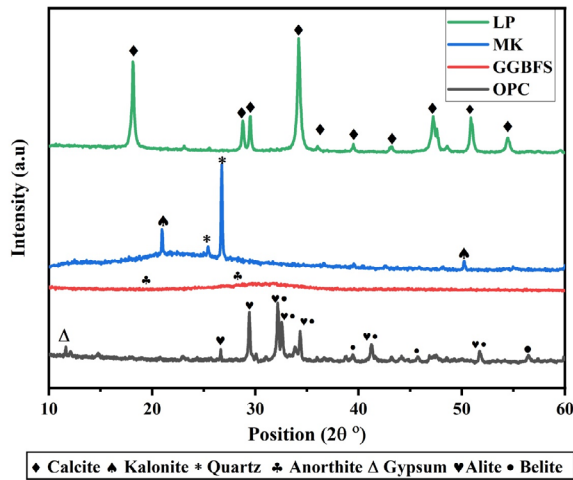


FIGURE 3. XRD patterns of raw binder materials.

2.2. Experimental design - Taguchi's approach

The experimental investigation conducted by Xavier et al. (28) on the ternary blended concrete system, which is rich in iron, was developed using the Taguchi method. Using the Taguchi approach, Guo et al. (29) developed experiments to examine cemented sand and gravel's freezing resistance and pore struc-

tural properties. Rahim et al. (30) employed the Taguchi technique to determine the best mix proportion of high strength concrete subjected to elevated temperatures to obtain the highest residual compressive strength. Tan et al. (31) used the Taguchi approach to optimize the unconfined compressive strength of admixture-reinforced grouts using fly ash, bentonite, and silica fume as binders in their study.

Design of experiments was employed to progress an experimental method for determining the optimum mix proportion of binders to produce synthetic aggregates. Specifically, the Taguchi method was preferred to optimize the binder content and water to binder ratio to produce durable synthetic aggregates.

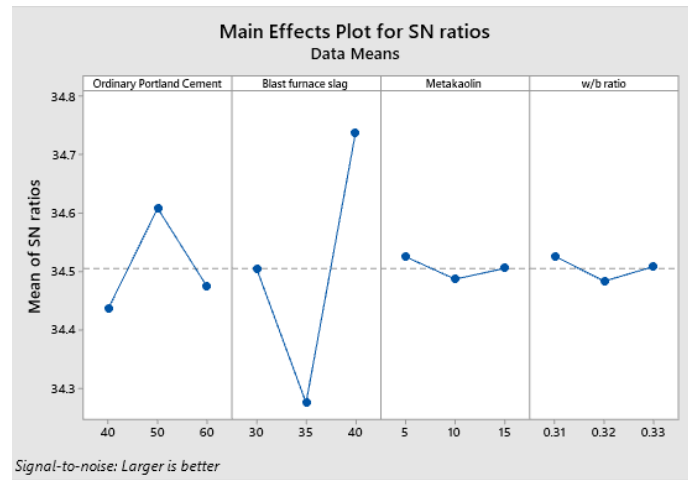


FIGURE 4. Optimized mix proportion by using Taguchi experimental design.

TABLE 3. Selected factors and their appropriate levels in Taguchi experimental design.

Factors	OPC (A) (%)	GGBFS (B) (%)	Metakaolin (C) (%)	w/b ratio (D)
Level 1	40	30	5	0.31
Level 2	50	35	10	0.32
Level 3	60	40	15	0.33

TABLE 4. A three-level L9 (3⁴) Orthogonal array.

Mix ID	Factors with their respective codes and actual levels (%)							
	OPC (A)		GGBFS (B)		Metakaolin (C)		w/b ratio (D)	
	Codes	Level	Codes	Level	Codes	Level	Codes	Level
TM1	A1	40	B1	30	C1	5	D1	0.31
TM2	A1	40	B2	35	C2	10	D2	0.32
TM3	A1	40	B3	40	C3	15	D3	0.33
TM4	A2	50	B1	30	C2	10	D3	0.33
TM5	A2	50	B2	35	C3	15	D1	0.31
TM6	A2	50	B3	40	C1	5	D2	0.32
TM7	A3	60	B1	30	C3	15	D2	0.32
TM8	A3	60	B2	35	C1	5	D3	0.33
TM9	A3	60	B3	40	C2	10	D1	0.31

As shown in Table 3, the selection of parameters and their appropriate levels was decided from prior studies. In this research, the four design factors: Ordinary Portland cement content (%), GGBFS content (%), metakaolin content (%), and w/b ratio, were considered with three levels, which makes a maximum of nine trials. By Taguchi's experimental design, the L9 (3^4) orthogonal array (as depicted in Table 4) was employed for this experimental investigation.

2.3. Synthetic aggregates production

Synthetic aggregates were produced using quaternary binders with optimized proportions, as shown in Figure 4. According to ASTM C305-06 (32) a mortar mixer consisting of a planetary motion mixing paddle with a microprocessor-based speed and program controller was used in the manufacturing of synthetic aggregates. The quaternary blended mixture of 50% ordinary Portland cement, 40% ground granulated blast furnace slag, 5% Metakaolin, and 5% lime powder was mixed for two minutes at a lower rotational speed of 140 rpm in a mortar mixer. The fine aggregate is combined to the binder mixture and blended well approximately 2 Min. Then, the dry blend was wetted with about 80 % of the required water combined with a high-range water reducer and allowed to mix for 2-3 min. A linear type of synthetic polypropylene fiber (PPF) was dispersed in the mixture at 0.3% of the total binder content. Then the remaining 20% of superplasticizer mixed water

was poured to the mixture, which was then agitated for an additional 1 Min. The sides of the mixing bowl were scraped and retained for 90 seconds. After a small resting, the mixture was mixed for 30 seconds at a higher rotational speed of 285 rpm. When a homogeneous mix has been formed, the prepared mortar mixture was poured into various shaped silicone mould and left to dry for 24 hours. As illustrated in Figure 6, four distinct shapes and sizes of synthetic aggregates were manufactured, including 10 mm cubical-shaped aggregates, 12 mm pyramid-shaped aggregates, 14 mm elliptical-shaped aggregates, and 16 mm frustum-shaped aggregates. Synthetic aggregates were taken from their moulds and cured at room temperature (28 °C) until their various properties were evaluated. Finally, hardened aggregates was sieved into appropriate sieve fractions in accordance with ASTM C330 grading specifications (33). Figure 5 depicts the production method of synthetic aggregates. As indicated in Table 5, except for the control mix, all the mixtures were prepared with the incorporation of polypropylene fibers. The control mix is the gauge mix to compare with the optimized mix. We have produced two compositional aggregates. One is Synthetic aggregates (SA) made with an optimized mortar mix (OM). Another one is Fiber Intruded Synthetic aggregates (FISA), which are also made up of optimized mortar mix along with the incorporation of polypropylene fibers. We have compared the results of produced SA and FISA with Natural coarse aggregates (NA) obtained naturally from rocks in section 3 and 4.



FIGURE 5. Manufacturing process of synthetic aggregates.

2.4. Testing

Physical properties such as bulk density, water absorption and specific gravity, mechanical properties such as crushing value, impact value, abrasion value and soundness value, and durability properties such as soundness value of produced synthetic aggregates were evaluated as described in the subsequent sub-sections.

2.5. Physical properties of synthetic aggregates

The loose and bulk density of the aggregates was estimated by a cylindrical mould of a distinct volume using the below given Equations [1] and [2], respectively. As per codal provision ASTM C127 (34), the results were taken for a water absorption test after 24 hours of soaking is inappropriate for porous nature aggregates. Using Equation [3], the amount of water absorbed by aggregates has been computed. For the mass measurements, dry oven samples, surface saturated dry samples, and fully saturated water samples were employed to obtain the oven-dry specific gravity of synthetic aggregates using Equation [4] as per ASTM C 127 (34).

$$D_l = \frac{w_1}{v} \quad [1]$$

$$D_c = \frac{w_2}{v} \quad [2]$$

Where: D_l = loose bulk density (kg/m^3); D_c = compacted bulk density (kg/m^3); w_1 = weight of loose aggregates (kg); w_2 = weight of compacted aggregates (kg); v = cylinder mould volume (m^3).

$$W = \left(\frac{w_s - w_o}{w_o} \right) \times 100 \quad [3]$$

Where: W = water absorption (%); w_s = dry weight of the surface saturated aggregate (g); w_o = oven dry weight of the aggregate (g).

$$Gsb = \frac{w_o}{(w_s - w_w)} \quad [4]$$

Where: Gsb = Bulk specific gravity; w_o = the oven dry weight of the aggregate (g); w_s = dry weight of the surface saturated aggregate (g); w_w = weight of aggregate in water (g).

2.6. Mechanical properties of synthetic aggregates

Generally, aggregate crushing value test (ACV) was conducted to determine the capability of coarse aggregates to withstand the force under applied loads. According to BS 812-110 (35). The crushing value was represented in a numerical index by using Equation [5]:

$$ACV = \left(\frac{M_2}{M_1} \right) \times 100 \quad [5]$$

Where: M_2 = mass of test sample passed through 2.36 mm sieve after crushing testing (g); M_1 = mass of test sample taken initially (g).

The aggregate impact value test (AIV) measured the synthetic aggregate resistance to rapid impact loads. This impact value test was done per the IS 5640-1970 (36) and BS 812-112 (37) test procedures. The Equation [6] is used to determine the aggregate impact value as given below:

$$AIV = \left(\frac{M_2}{M_1} \right) \times 100 \quad [6]$$

Where: M_2 = mass of test sample passed through 2.36 mm sieve after impact testing (g); M_1 = mass of test sample taken initially (g).

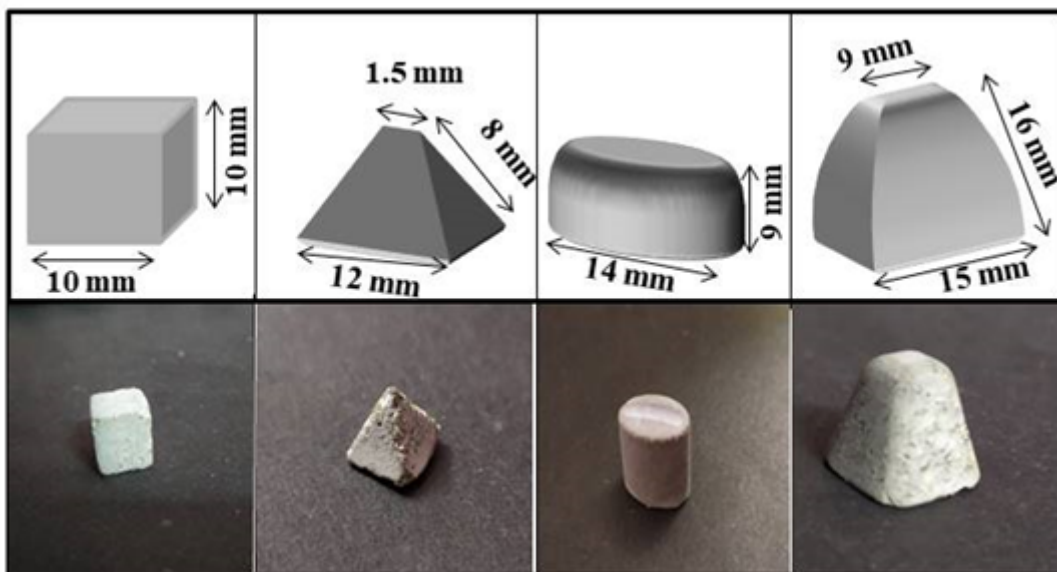


FIGURE 6. Produced Synthetic aggregates in various shape and sizes.

According to IS: 2386 -1963 (Part IV) (38), the aggregate abrasion test value (AAV) test has been conducted to determine the abrasion resistance of synthetic aggregates. The aggregate abrasion value was determined by following Equation [7]:

$$AAV = \left(\frac{M_2}{M_1} \right) \times 100 \quad [7]$$

Where: M_2 = mass of test sample passed through 1.7 mm sieve after abrasion testing (g); M_1 = mass of test sample taken initially (g).

2.7. Durability properties of synthetic aggregates

The aggregate soundness value (ASV) test was performed to determine aggregates' durability and evaluate the resistance to disintegration under extreme weather conditions. For this test, synthetic aggregates shown in Figure 7 were submerged in a 15 mm depth of sodium sulphate solution for 18 hours. Then the samples were taken from the sulphate solution and allowed to fully drain for 15 minutes before being placed in the drying oven. Afterwards, the oven was switched to initiate a drying process to attain uniform mass. After removing the aggregates from the oven, they were allowed to cool at room temperature. The dried coarser material was sieved with an 8 mm sieve to determine the mass loss. This percentage of mass loss is termed as soundness value, and it was computed by using Equation [8] This procedure was conducted as per IS 2386 -1963 (Part V) (39).

$$ASV = \left(\frac{M_2}{M_1} \right) \times 100 \quad [8]$$

Where: M_2 = mass of sample passing through 8 mm test sieve after the soundness test (g); M_1 = mass of test sample taken initially (g).

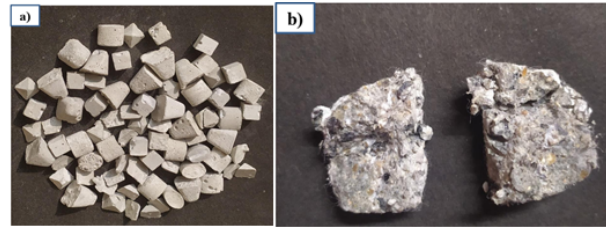


FIGURE 7. (a) External appearance (b) Core structure of produced fiber intruded synthetic aggregates.

2.8. Compressive strength testing

Compressive strength testing has been performed to evaluate the hydration effect on quaternary binders. In accordance with ASTM C109 (36), a 50 mm cube mould was used to cast mortar cubes. Then the set of designed experimental trial mixtures of the produced mortar samples was tested for compressive strength, as presented in Table 5.

2.9. Micro hardness testing

In this work, the micro-hardness testing was conducted to examine the surface properties of the produced aggregates. The samples of natural aggregates (NA), manufactured synthetic aggregates (SA), and fiber-intruded synthetic aggregates (FISA) were preferred for this test. The test sample was prepared with dimensions of 10 mm x 10 mm x 2 mm slices. Initially, these samples were ultrasonically cleaned in acetone. After the sample was fully dried, it was polished to produce a smooth, glossy surface to identify indentation locations easily. The micro-hardness value was obtained by indenting the sample at distance intervals of 10 μ m over the aggregate surface by applying a force of 10 g for 10 seconds using a Vickers micro-hardness tester as shown in Figure 8.

TABLE 5. Mixture (kg/m³) design for synthetic aggregate production.

Mixture	OPC (kg/m ³)	GGBFS (kg/m ³)	MK (kg/m ³)	LP (kg/m ³)	Sand (kg/m ³)	Water (kg/m ³)	w/b ratio	SP (kg/m ³)	PPF (kg/m ³)
CM	740	0	0	0	2035	230	0.31	1.1	0
TM1	296	222	37	37	2035	230	0.31	1.1	1.78
TM2	296	259	74	37	2035	237	0.32	1.1	2.00
TM3	296	296	111	37	2035	245	0.33	1.1	2.22
TM4	370	222	74	37	2035	245	0.33	1.1	2.11
TM5	370	259	111	37	2035	230	0.31	1.1	2.33
TM6	370	296	37	37	2035	237	0.32	1.1	2.22
TM7	444	222	111	37	2035	237	0.32	1.1	2.44
TM8	444	259	37	37	2035	245	0.33	1.1	2.33
TM9	444	296	74	37	2035	230	0.31	1.1	2.55
OM	370	296	37	37	2035	230	0.31	1.1	2.22

Note: CM-Control mix, OM- Optimized mix, SP- Super plasticizer, PPF- Polypropylene fibers.

2.10. Microstructural analysis

Utilizing X-ray fluorescence spectroscopy (XRF), the chemical composition of the raw binders was analyzed as shown in Table 2. Bruker model S8 Tiger X-ray spectrometer was used to assess binder mineral phases and oxide percentages. This spectrometer has SPECTRA plus software for qualitative and quantitative element identification. The powder X-ray diffraction technique was executed using a Bruker D8 advanced model powder X-ray diffractometer to detect the phase change of raw materials and produced synthetic aggregates.

Scanning Electron Microscopy (SEM) along with Energy Dispersive X-ray spectroscopy (EDX) has been performed to establish the morphological properties of produced synthetic aggregates. ZEISS EVO 18 model scanning electron microscope from Carl Zeiss Microscopy is employed to examine the microstructure of produced synthetic aggregates. FTIR spectroscopy was used to detect the incremental stages generated through the hydration effect of cement and mineral admixtures. Using a Shimadzu make IRAffinity-1 model FTIR spectrophotometer, the peaks of hydrated aggregate samples are observed. It has a wavelength limit of 4000-400 cm^{-1} . After 28 days of hydration, a spec-

tral comparison was conducted between the control and optimized mixture. This comparison enables the determination of the absorption spectrum and the identification of unknown compounds in various mixtures

TA instruments USA's SDT Q600 thermo-gravimetric analyzer was employed to determine the quantitative mass loss of produced synthetic aggregates. This technique establishes the relationship between bound water and the degree of hydration at an earlier stage. A powdered aggregate sample was soaked for 48 hours in ethanol to prevent further hydration. The samples were placed in an oven with hot air to prevent the produced aggregate specimens from being hydrated. TGA was conducted using the temperature ramp of 20°C till 800°C at an amount of 20°C/min in an inert N_2 gas flow chamber.

Atomic Force Microscopy (AFM) is a faster scan probe microscopic technique used to visualize the topography of a sample surface. Topographic images are acquired with the help of a probe with a sharp point at the end of a cantilever. The cantilever tip moves across a specimen's surface. As the tip contacts the specimen's surface, its deflection is measured, and the surface's topography is recorded. 2D and 3D scans of AFM images are recorded.

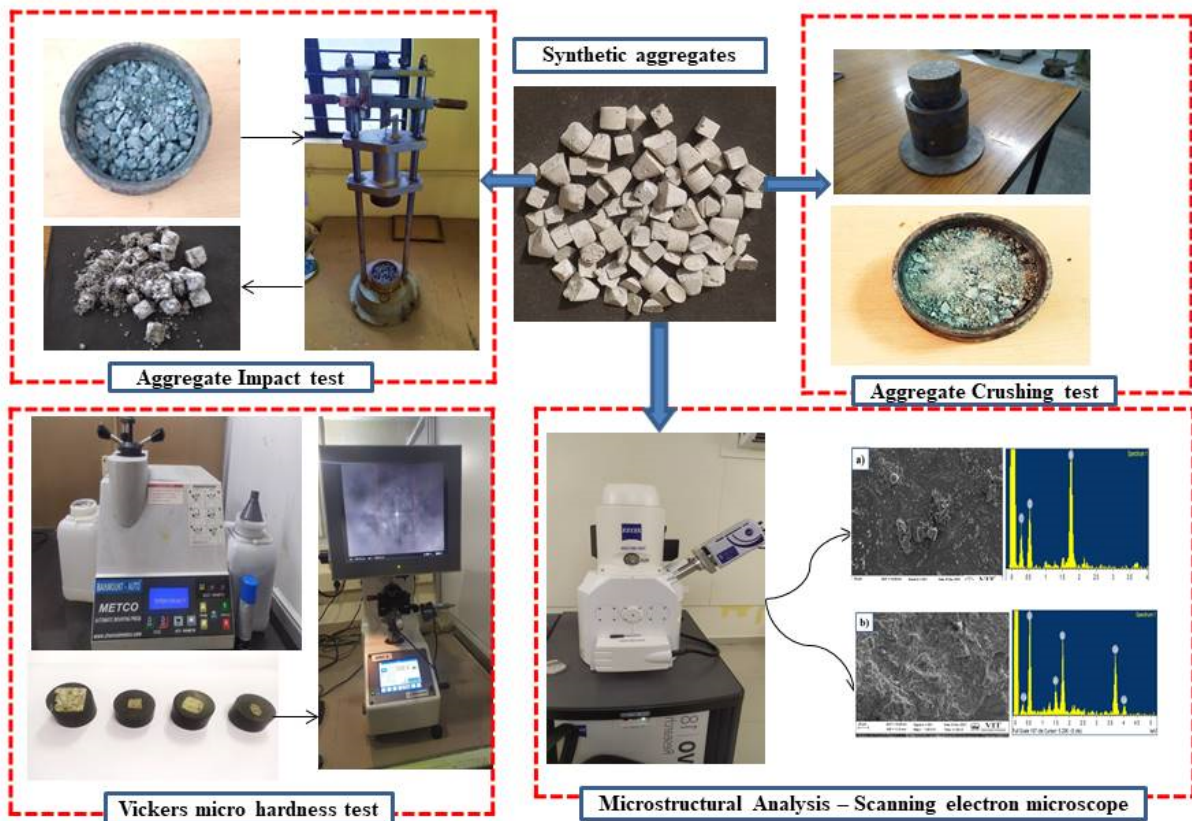


FIGURE 8. Pictorial representation of several tests conducted on produced synthetic aggregates.

3. RESULTS AND DISCUSSION

3.1. Compressive strength

Trial experiments were performed to identify the control factors and their levels in the Taguchi technique. According to ASTM C109 (40), mortar cube compressive strength was measured from nine trail mixes and an optimal mix designed using Taguchi's experimental design. From the control factors listed in Table 3, the main effects of S/N ratios were determined based on the "Larger is Better" condition (as depicted in Figure 4) bestowed by Taguchi, where the compressive strength is higher for the optimized mix. The test results of compressive strength of the control mixture gained after 7 and 28 days of curing are 30 and 34 MPa, respectively. The results suggested that the compressive strength of the mortar made for aggregates improved with the length of its curing age. The increased GGBFS content enhanced the strength of mortar at 28 days rather than 7 days. This strength represented that the GGBFS, at an early age, showed the lowest strength and enhanced the strength of later-aged mortar. The used binders including GGBFS, Metakaolin, and lime powder chemically reacted with one another and produced C-S-H gel, which enhances the compressive strength after 28 days of curing (41). According to Figure 4, the optimal values for the parameters were Ordinary Portland cement (50%), Ground granulated blast furnace slag (40%), Metakaolin (5%), and w/b ratio (0.31), resulting in the optimized mixture having a highest compressive strength of 36 MPa at a curing period of 28 days. The control mix comprised mortar made only with OPC as a binder and, according to the Taguchi orthogonal array experimental design ($L_9(3^4)$), comprised nine initial experimental mixes. This is revealed in Table 5, and they are labeled as TM1 to TM9. According to the mix proportions calculated in Table 5, the mortar cube samples (50mm x 50 mm x 50 mm) were cast. Six mortar cubes were cast for each trail mix (TM1 to TM9) including the control mix and kept in the curing for 28 days. Totally, 60 mortar cubes were cast for nine trail mixtures and control mix. According to ASTM C109 (40), three mortar cube samples were tested for compressive strength testing at 7 days, and the remaining three mortar cube samples were kept and then tested at the age of 28 days. The average measured values of tested mortar cube samples were noted. This has been plotted in Figure 9. Taguchi optimization analysis was carried out on the compressive strength of 9-nine trail mixes. After that, the "Larger is better" condition was used to obtain maximum compressive strength, yielding one ideal mixture distinct from the above nine trail mixtures. This mix is termed an optimized mix (OM), as shown in Figure 4. After that, six mortar cubes were cast again to confirm the optimized mix and tested compressive strength for 7

and 28 days. The obtained the maximum compressive strength of 36 MPa at 28 days, higher than the control and trail mixtures, as shown in Figure 9.

The mortar mixture optimized from cubes was used to manufacture synthetic aggregates in four different shapes and sizes, as shown in Figure 6, and cured for 28 days. As depicted in Figure 7(a), the physical, mechanical, and durability properties of manufactured synthetic aggregates of well-graded (equivalent combination of four various shapes and sizes) were tested. The mean values of test results were recorded at the age of 28 days.

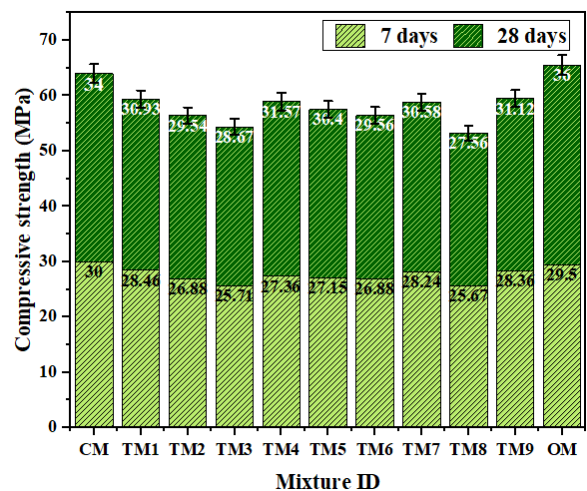


FIGURE 9. Compressive strength of trail and optimized mixtures of mortar cubes at 7 and 28 days.

3.2. Bulk density

Generally, the bulk density is used to estimate the unit weight of concrete as well as to access the dead weight of structural concrete. After 7 days of curing the aggregate samples, the densities of both natural and synthetic aggregates were determined as shown in Figure 10a. The loose bulk density of synthetic aggregates (SA) and fiber intruded synthetic aggregates (FISA) fall between 1100 and 1250 kg/m³. While the density of FISA was measured at 1146 kg/m³, it met the requirement that such density of lightweight aggregate be below 1200 kg/m³ according to BS EN 13055-1 (42). Table 6 shows that FISA is lighter than synthetic aggregates (SA). This lightweight is due to the inclusion of fibers in FISA, and its aggregate density was lower than that of SA. The degree of compaction and the presence of voids are determined by aggregates different size and shapes, which considerably influence the rod-ded bulk density of aggregates. Artificial aggregates produced prior to this investigation have densities between 1170 and 1330 kg/m³ (43-45). The addition of cement, which has higher specific gravity than GGBFS, is responsible for the increased density of produced synthetic aggregates (44). Also, a compar-

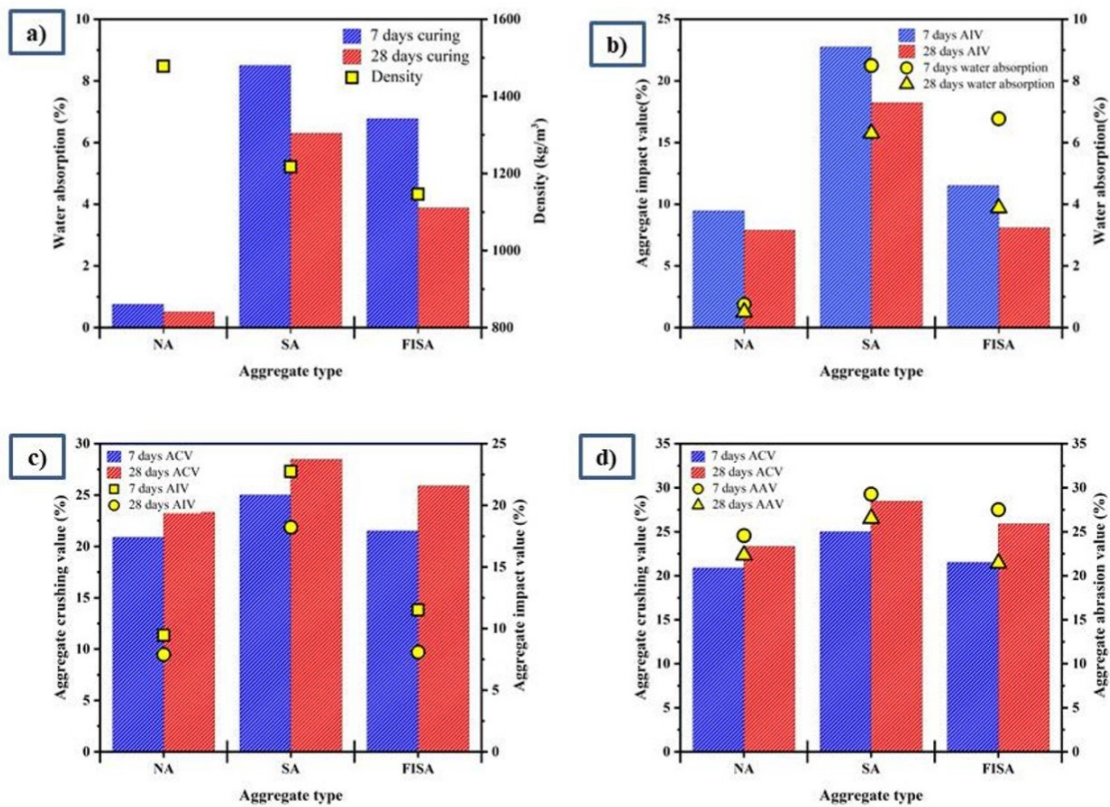


FIGURE 10. Correlation between (a) Water absorption and density (b) Aggregate impact value and water absorption (c) Aggregate crushing and impact value (d) Aggregate crushing and abrasion value.

TABLE 6. Physical properties of natural aggregates and produced synthetic aggregates.

Type of aggregate	Bulk density (kg/m ³)	Water absorption (%)		Specific gravity	Fineness modulus
		7days	28 days		
NA	1478	0.75	0.5	2.74	7.16
SA	1217	8.5	6.3	2.56	7.31
FISA	1146	6.77	3.88	2.52	7.31

Note: NA- Natural aggregate, SA- Synthetic aggregate, FISA-fiber intruded synthetic aggregate.

ison between synthetic aggregates (SA) and natural aggregates (NA) revealed that SA (1217 kg/m³) had much lower densities than NA (1478 kg/m³). The aggregates with the highest and lowest densities were produced by synthetic aggregates (SA), and fiber intruded synthetic aggregates (FISA), which were 17.67% and 22.46% lighter than natural aggregates (NA), respectively.

3.3. Water absorption

After three days of immersion in water, natural and synthetic aggregates were subjected to a water absorption test. Similarly, a water absorption test

after the completion of 7 days and 28 days of curing period is reported in Table 6. The water absorption capabilities of produced SA were determined to be within the usual limit of less than 25% after 7 days of curing specified by ACI 213R (46). The absorption test results of 28 days revealed that the decrease in water absorption of SA and FISA with the continuous hydration of specimens resulted in the formation of a sufficient amount of hydration products. The XRD analysis further confirmed these hydration products. Hydrated cement products made a further pozzolanic interaction between GGBFS and metakaolin, developing more amount of calcium-silicate-hydrate (C-S-H) products, which leads to a denser microstructure (44). The produced syn-

thetic aggregates can also be compared to the naturally occurring aggregates, which have a very lower water absorption rate of 0.75%. However, the water absorption of manufactured SA and FISA was higher than that of commercially available natural aggregates after 7 days of curing, according to the current investigation. As depicted in Figure 8b, water absorption values decreased significantly as curing period was extended from 7 to 28 days. Numerically, water absorption at 28 days of curing was decreased by 25.88% and 42.69% compared to 7 days of curing for SA and FISA samples, respectively. SA aggregates are more porous than FISA aggregates. In prior investigations, paper ash (47), waste concrete powder (48), fly ash (49), slag (50), concrete slurry and fine incineration bottom ash (51), and other raw materials were employed to produce artificial aggregates. However, it was noted that several aggregates were deficient in showing the required strength and had a higher water absorption rate. While the aggregates developed in this research, namely SA and FISA, exhibited comparatively high strength and low absorption of water (6-9%) that are useful for real-time applications. However, it has been observed that the performance of fiber intruded synthetic aggregate can be greatly enhanced by utilizing polypropylene fibers during production, achieving the lowest water absorption of 3.88 %.

3.4. Specific gravity

The aggregate specific gravity is the proportion of the aggregate weight to the weight of water for the same volume. The specific gravity of the manufactured synthetic aggregate (SA) and the fiber-intruded synthetic aggregate (FISA) is 2.56 and 2.52, as shown in Table 6. It was found to be nearer to the specific gravity of natural aggregates. Hence, the produced synthetic aggregates belong to weight of natural aggregates. Due to the increase in GGBFS content, the specific gravity of produced synthetic aggregates increased. Spherical fly ash particles adhere to one another during the pelletization process and retain a certain number of voids, leading to the

lower specific gravity of the pellets. The low specific gravity and increased water absorption form porous aggregates (51).

3.5. Aggregate crushing value

The aggregate crushing value (ACV) test was performed to evaluate the strength of aggregate. The test of aggregate samples of results obtained for 7 days and 28 days of curing as illustrated in Figure 8c. It was noted that the crushing value results of FISA are similar to the findings of impact value test results. It reveals that adding fibers improved the crushing value of the aggregate. ACV development after 28 days of curing was 13.84% for SA aggregates and 20.37% for FISA aggregates, respectively. It is important to observe that the difference in ACV between aggregates cured for 7 and 28 days was more than the improvement in impact resistance, indicating that aggregates were more resistant to compressive loads than impact loads. FISA aggregates performed better than SA aggregates in terms of strength gain over time. In addition, ACV test results were aligned with density and impact value test results. The strength of manufactured synthetic and natural aggregates was also compared. As illustrated in Figure 11, visual observations were also taken for natural and produced synthetic aggregates after crushing.

3.6. Aggregate impact value

The aggregate impact value (AIV) is a measurement of an aggregate resistance to a sudden impact or shock. It is different from its resistance to a progressively applied compressive force. AIV of both natural and produced SAs was performed, and the setup was shown in Figure 12. The aggregate impact value of natural and synthetic aggregates gained 8.08 % and 18.22 %, respectively. Obviously, the inclusion of lime content increases the impact resistance of SA and FISA aggregates and densifies the microstructure of aggregates. This impact strength was owing to the enhanced production of C-S-H,



FIGURE 11. Visual appearance after crushing test (a) NA (b) SA (c) FISA.

calcium hydroxide ($\text{Ca}(\text{OH})_2$) and portlandite (CH) as a result of an increased hydration process (13). Additionally, cement reacts with CaO , present in GGBFS, and activates it for strengthened aggregate at micro level (52). On the other hand, GGBFS and MK react with CH present in cement and stimulate strength development. A comparative graph of water absorption with aggregate impact value is shown in Figure 10b. It can be noted from Figure 10b, that aggregate impact value and water absorption have an inverse relation. As shown in Figure 10b, SA and FISA exhibited a good correlation between aggregate impact value and water absorption values. Thus, aggregates with less amount of water absorption possess greater impact resistance. After 28 days, the AIV of produced SA and FISA aggregates was within the permissible limit (less than 30%) as specified by BS-812-112 (37). Similarly, SA aggregates containing greater GGBFS offered high impact resistance, reduced porosity, and significantly improved strength (53). The natural aggregates had an aggregate impact value of only 7.89%, much lower than all developed synthetic aggregates.



FIGURE 12. Aggregate Impact test apparatus.

3.7. Aggregate abrasion value

The percentages of abrasion values at 28 days of curing for natural (NA) and synthetic (SA) aggregates are 22.34% and 26.51%, respectively. As shown in Figure 10d, fiber intruded synthetic aggregates (FISA) have the lowest percentage of abrasion value (21.42%) conducted at 28 days. This indicated that these aggregates have a good abrasion resistance due to the inclusion of polypropylene fibers. The maximum material loss for aggregates intended for the pavement layer is 40%. As a result of these findings, FISA and SA can be used as structural ma-

terials for applications of lightweight structural concrete requiring a high level of wear resistance and mechanical performance (53).

3.8. Vickers micro hardness test

Figure 13 compares the micro hardness of natural aggregate (NA), synthetic aggregate (SA), and fiber-introduced synthetic aggregate (FISA). For all three samples, the micro hardness was observed to be constant up to a surface distance of 40 μm . After that, the micro-hardness value was observed to be increased around the distance of 40–60 μm on the aggregate surface and remained constant. While comparing the micro-hardness value of SA and FISA samples, it was observed that the SA sample had a lower micro-hardness value up to 40 μm . This low-level micro hardness is due to micro-level cracks and pores presented in synthetic aggregates (54).

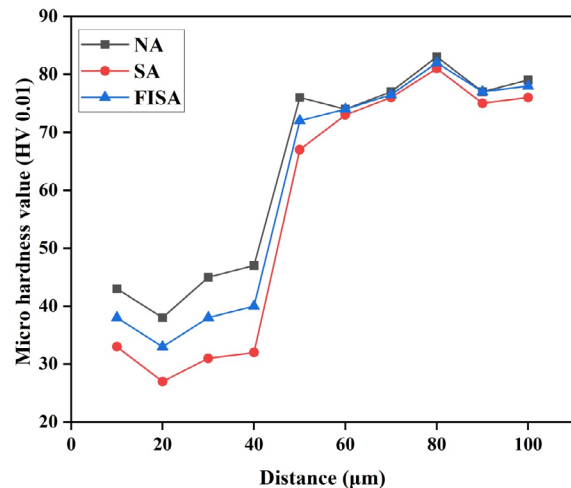


FIGURE 13. Vickers micro hardness of natural and produced aggregates.

3.9. Aggregate soundness value

The soundness test was conducted to measure an aggregate's resistance to weathering and freeze-thaw cycles-induced disintegration. The soundness values of natural and synthetic aggregates were 0.996 % and 1.843 %, respectively. Thus the results suggest that, despite their relatively high water absorption, the manufactured synthetic aggregates met ASTM C 330 (33) standards for a concrete aggregate without causing any soundness defects.

3.10. Significance of shape parameters for produced aggregates

The size and shape of aggregates immediately impact the binder requirement, workability, concrete

strength, durability, and cost of concrete. Usually, natural aggregates with angular shapes were used for concrete production. Generally, rounded, elongated, and flaky aggregates provide superior workability but lower in bond strength and mechanical properties. Hence, we have preferred four distinct shapes cubical (10 mm), pyramid (12 mm), elliptical (14 mm), and frustum (16 mm). Cubical aggregate has flat surfaces in all directions. An aggregate with a pyramid shape comprises clearly defined edges formed at the junction of a nearly flat surface. Elliptical-shaped aggregates have the smallest surface area and require less cement paste for bonding than other shapes. Frustum-shaped aggregates have more surface area and require more cement paste for bonding. Three tests, Aggregate Impact value (AIV),

Aggregate Crushing value (ACV), and Aggregate Abrasion value (AAV) were conducted to measure the toughness of natural and synthetic aggregates with an equal combination of four geometric shapes, as explained in 3.4 to 3.7.

4. MICRO STRUCTURAL INVESTIGATION

4.1. Scanning electron microscopy

Figure 14 illustrates the SEM pictures of the raw binders utilized in this examination. Magnification of 500X was used in SEM analysis. The EDX spectra of aggregate samples were acquired from the

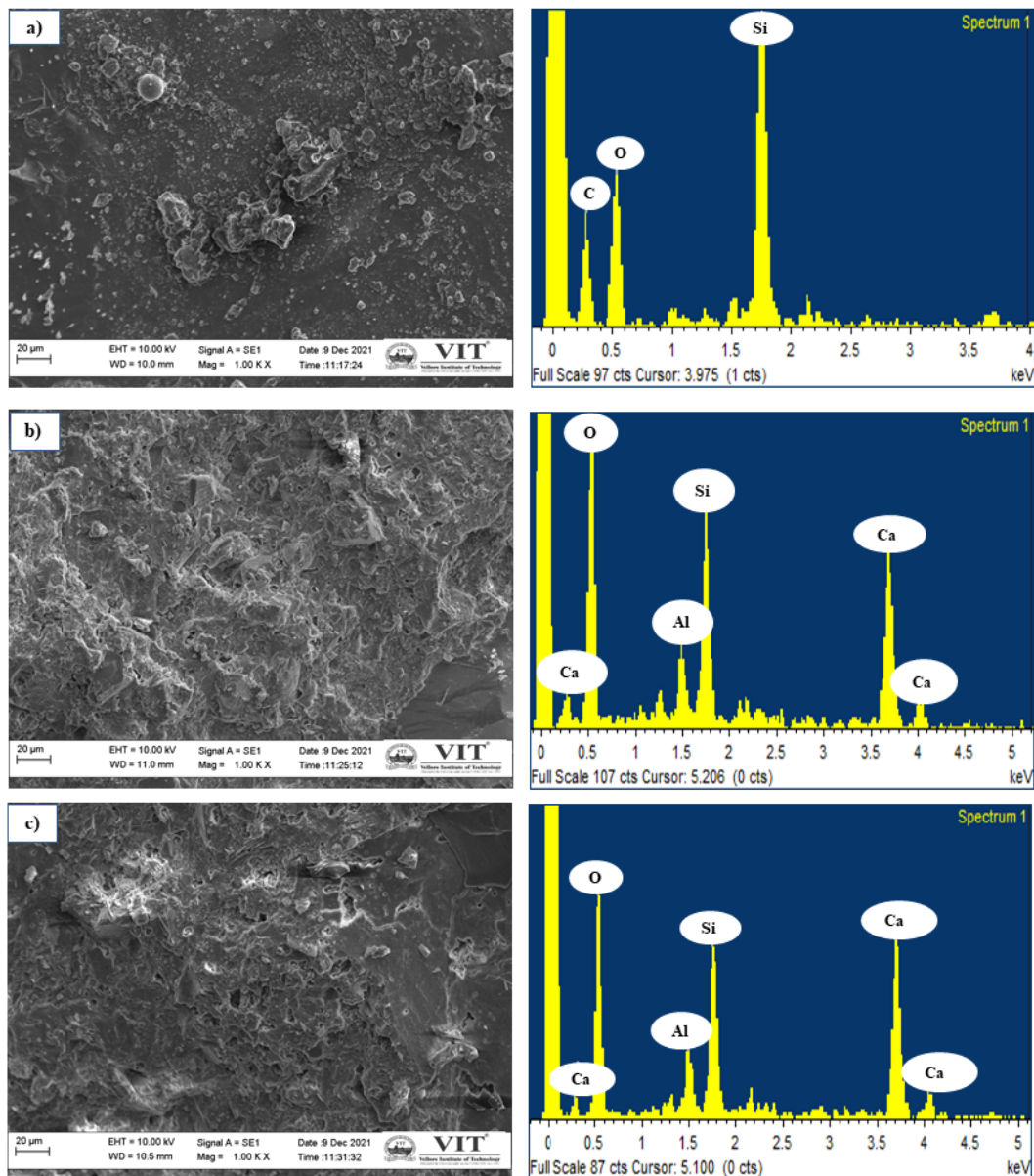


FIGURE 14. Morphological view of (a) Natural aggregates (b) Synthetic aggregates (c). Fiber intruded synthetic aggregates.

entire region of images taken from SEM, as shown in Figure 14. SEM images of natural aggregates are shown in Figure 14(a). The SEM/EDX examination revealed the distinctive morphological characteristics of the produced synthetic aggregates. The EDX measurements reveal that silica and calcium are more prevalent minerals in the natural aggregate, indicative of sedimentary rock. C–S–H is the primary product of cement hydration and a crucial role in the strength of cement and other products formulated from cement. Due to the usage of mineral admixtures, EDX obtained results demonstrated clearly that the change of components occurred in the SA and FISA. Figure 14(b) depicts increased C–S–H formation. The Synthetic aggregates had greater pores at the age of 7 days of curing, and the volume of pores was reduced after 28 days of curing. Due to the pozzolanic interaction between slag and metakaolin, cement mortar densifies at later ages. Figure 14(c) indicates that adding polypropylene fibers decreased the porosity and micro-cracks of fiber intruded synthetic aggregates.

4.2. X-ray diffraction

Using X-ray diffraction (XRD), the compositional changes (increase) of NA, SA, and FISA samples were studied. Figure 15 illustrates the XRD patterns for NA, SA, and FISA. The montmorillonite ($\text{Al}_2\text{H}_2\text{O}_{12}\text{Si}_4$), Anorthite ($\text{CaAl}_2\text{Si}_2\text{O}_8$), Calcium aluminosilicate ($\text{Ca}_2\text{Al}_2\text{SiO}_7$), Lawsonite ($\text{CaAl}_2\text{Si}_2\text{O}_7(\text{OH})_2 \cdot \text{H}_2\text{O}$), Quartz (SiO_2) and Calcite (CaCO_3) peaks were identified for NA, SA, and FISA as shown in Figure 15. Based on the XRD results of SA and FISA samples, it was determined that the enhanced strength of the both samples is due to the development of calcium aluminosilicate (55). In addition, Anorthite peaks indicated that GGBFS reacted with metakaolin and lime powder. Adding lime powder in SA and FISA reduced the intensity of the quartz peak, as shown in Figure 15. The peaks support this result at 26.58° (2θ), where the quartz peak is prominently visible. Thus the SEM/EDX study results validated the strength enhancement in produced aggregates.

4.3. Fourier transform infrared spectroscopy (FTIR)

Fourier transform infrared spectroscopy (FTIR) was employed to discover an absorption of infrared spectrum, emission, and photoconductivity of produced synthetic aggregate with diverse functional groups. The Infrared spectra are typically measured between the range of 4000 and 400 cm^{-1} . The FTIR spectra of aggregate samples NA, SA, and FISA were shown in Figure 16. NAs were identified with

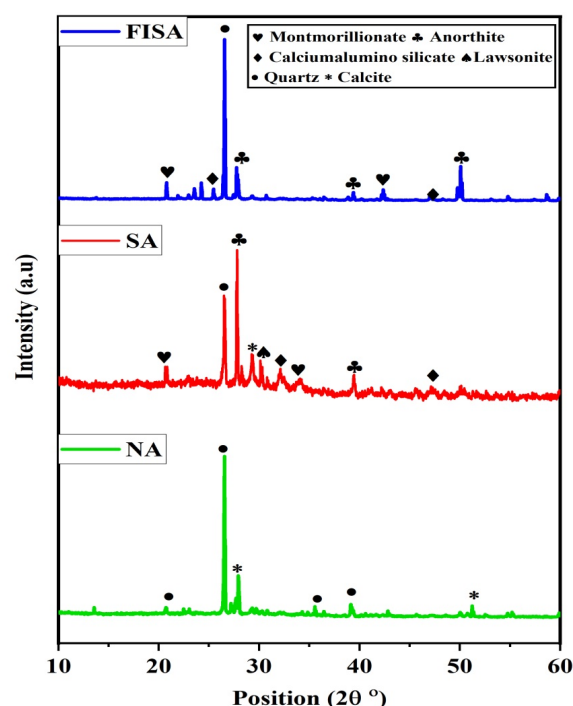


FIGURE 15. XRD patterns of natural (NA) and synthetic aggregates (SA, FISA).

prominent bands around 2343.51 cm^{-1} , 1431.18 cm^{-1} and 997.20 cm^{-1} , respectively. In SA, vibrations of 2335.80 cm^{-1} specified the occurrence of the C–H stretching group. Bands at 1431.18 cm^{-1} (C–O stretching group) indicate the presence of calcite at the site of formation of the principal crystalline phase. The signal at 997.20 cm^{-1} shows the presence of vibrations in the C–C skeleton. The bending vibration of –OH between 3250 and 3750 cm^{-1} is caused by the combination of structural and free water. It was observed that raw binders exhibit absorption maxima in this region, showing that these binders contain trace amounts of water. In contrast, free water presented in aggregates was absorbed on the surface and confined within the pores of reaction products. Aluminum (Al) availability in metakaolin enhanced the hydration level. Similarly, Al ions replaced Si ions presented in GGBFS to produce Si–O–Al, that restructured to develop efficiently organized aluminosilicates (56). The spectrum exhibits a significant broadband signal at 972.12 cm^{-1} , which results from the asymmetrical Si–O–Al stretching (57). Therefore, FTIR test results showed the structural reorganization occurred in aggregate samples (NA, SA and FISA).

4.4. Thermo-gravimetric analysis (TGA)

Thermo-gravimetric (TG) curves provide a very important indication of the temperature stability of the produced aggregate matrix. Figure 17 depicts im-

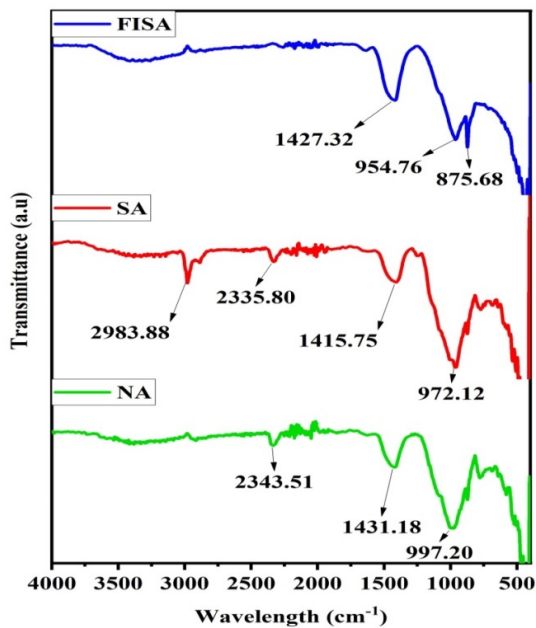


FIGURE 16. FTIR spectrums of natural aggregates and synthetic aggregates.

ages of the TGA of NA, SA, and FISA samples, respectively. Initially, an endothermic between 50 and 150°C was identified, resulting from the evaporation of water present in the synthetic aggregates produced with cementing binders. Consequently, the C-S-H presented in SAs could be estimated using the predicted mass losses derived from the TGA curves among 25°C as starting temperature and 125°C as ending temperature. From this observation, the corresponding mass losses of NA, SA, and FISA aggregate samples in this range were determined to be 4.983%, 4.723%, and 4.427%, respectively. This result showed that SA and FISA had a greater C-S-H concentration.

In addition, this occurrence shows that the pozzolanic reaction between GGBFS and MK enhances the strength properties of the manufactured SA and FISA. The results exposed that the strength properties of SA were less than those of FISA. The identical C-S-H contents of these samples are an interesting finding. In addition, TGA data showed that between 400 and 800°C, carbonates formed as in the temperature phase. Hence, the carbonate contents of SAs was determined using the mass losses obtained from the TGA plotted curves roughly in between 550°C as starting temperature and 625°C as ending temperature. The observed mass losses of NA, SA, and FISA samples between 550°C and 575°C were 1.846%, 1.548%, and 0.775%, respectively. According to these findings, the carbonate concentrations of SAs were near one another. In addition, it is established that the complete proportion of mass retained after heating to 700°C remains consistent

in all cases, indicating its thermal stability and the absence of any further thermal degradation.

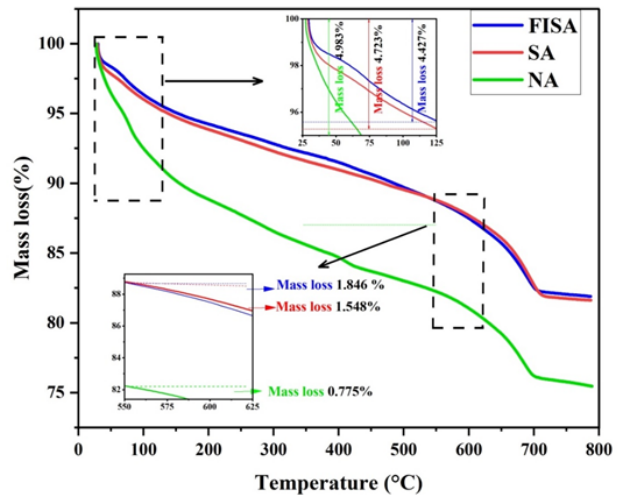


FIGURE 17. TGA curves of (a) natural and synthetic aggregates.

4.5. Atomic force microscopy

Using atomic force microscopy (AFM), aggregate surface roughness and multiple roughness parameters were determined. Figure 18 depicted 2D and 3D topographical images of produced synthetic aggregates. Darker parts suggested a relatively low topographical surface and in contrast lighter spots showed a higher topographical surface as observed in 3D topographical images as shown in Figure 18. Different roughness indices such as arithmetical mean deviation (S_a), root mean square deviation (S_q), maximum height deviation (S_v), maximum peak height deviation (S_p), maximum valley depth deviation (S_v) of NA, SA and FISA were presented in Table 7. It was observed that several roughness parameters of fiber intruded synthetic aggregate samples (FISA) were significantly improved compared to synthetic aggregates (SA). The improved average roughness (R_a) of FISA may have been caused by the coarser surface of the binder reaction products with fibers increased the surface area. Other FISA characteristic factors, including S_a , S_v , and S_p , were greater than SA. Also it favorably altered the topographical surface of produced aggregates including more prominent hills and valleys, resulting in the binder reaction products with a rough surface (58). Developing a harder, stronger, and more organized binder arrangement improved the actual contact area and enhanced binding, strengthening the mechanical and durability properties of the manufactured synthetic aggregates and fiber intruded synthetic aggregates.

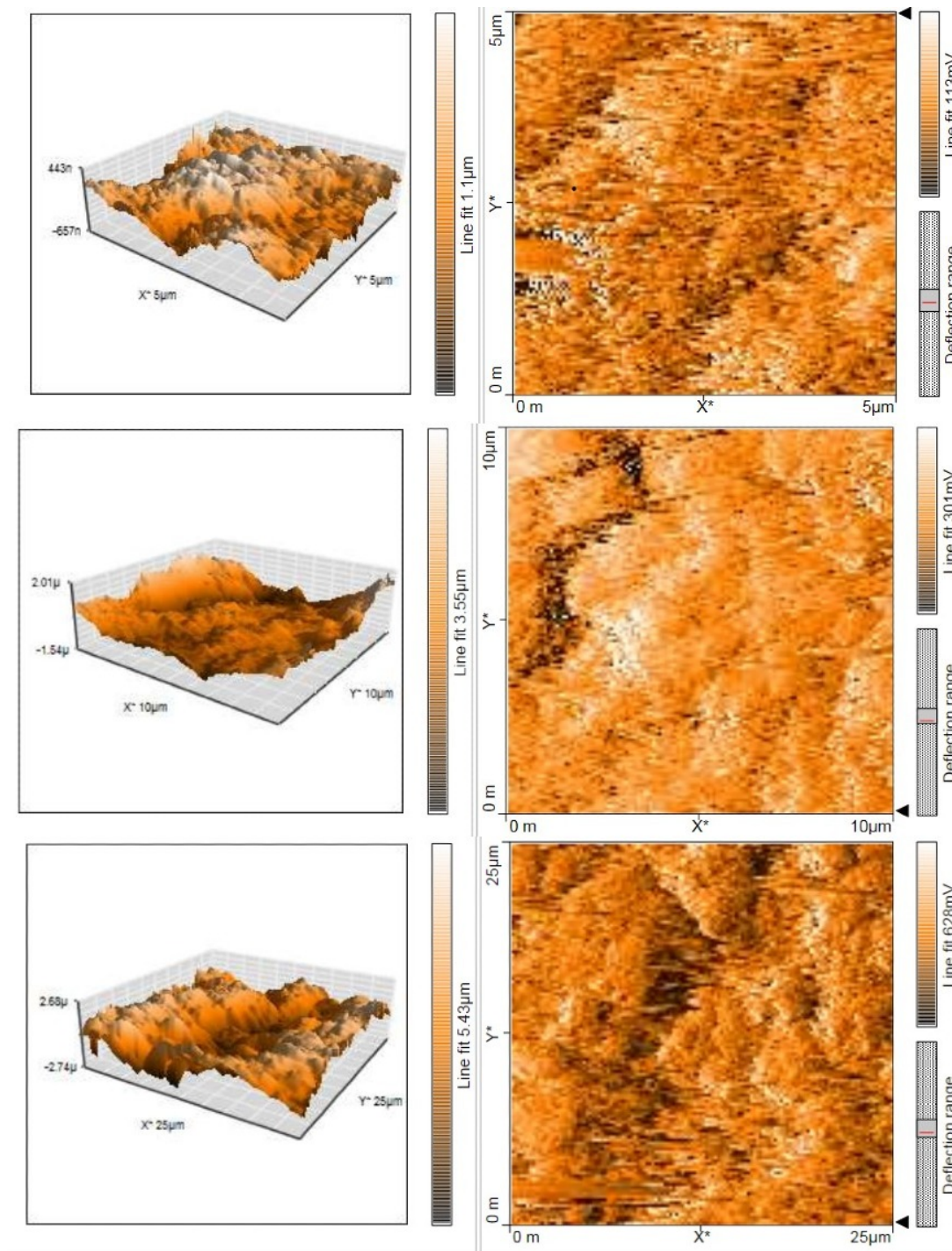


FIGURE 18. 2D and 3D topographical images of NA, SA, and FISA.

TABLE 7. Roughness distribution of natural and produced aggregates.

Sample ID	Surface area roughness Parameters						
	S_a (nm)	S_q (nm)	S_y (μm)	S_p (nm)	S_q/S_a	S_v (nm)	S_m (pm)
NA	730.49	869.34	4.944	2437.2	1.190	-2506.9	-10.026
SA	126.24	161.16	1.519	512.4	1.277	-1006.5	-10.028
FISA	394.73	520.02	3.627	2197.7	1.317	-1429.4	-10.028

4.6. Optical microscope

An optical microscope was used to analyse fractured synthetic aggregate surface morphology and microstructure. There was a noticeable change in morphology between the aggregate edges and interiors. The inside part was densely packed with pores ranging from 10 to 50 μm. Pores within the aggregate were frequently self-contained and detached from the outer surface. Moreover, SEM images reveal that the aggregate surface was not as smooth and resulting in a larger contact area between the binder particles, facilitating densely packed microstructure. The pores of synthetic aggregates were smaller than capillary voids, showing that lime powder leads to a reduction in pore dimensions as self-healing potential and an increased its C-S-H development, as shown in Figure 19.

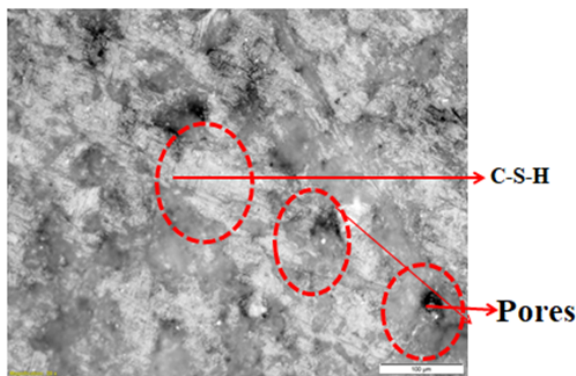


FIGURE 19. Optical Microscopic images of the fracture surface of synthetic aggregates.

5. ECONOMICAL AND ENVIRONMENTAL FACTORS ANALYSIS

5.1. Economical analysis

Table 8 provides an overview of the total costs incurred in India during the manufacturing and transport of essential materials used in the manufacturing of synthetic aggregates. In addition, water expenses are based on the cost of industrial purpose water, which is marginally more expensive than the domestic water. The costs of various mortar mixtures can be estimated using the proportions indicated in Table 5.

Figure 20 depicts the correlation between concrete strength and its production cost. It is abundantly clear

that the entire manufacturing cost of aggregate and the compressive strength of the mortar do not have a linear relationship. The cost usually varied depending on the quantity of cement that is required; if the proportion is high, then the cost is also increased. The control mixture, which contains no mineral admixtures as binders, has the highest cost of 94.82 dollars per cubic metre. While both target strength and cost are considered, the optimal mix is the best possible option for reaching a higher target strength at a minimal cost. Moreover, the GGBFS dosage of 40% has a significant impact on the cost of producing synthetic aggregates due to its low cost. Ultimately, it was clear that implementing the GGBFS would have positive effects on the economy, both directly and indirectly, in the form of benefits such as reduced disposal costs and improved dependability of waste management.

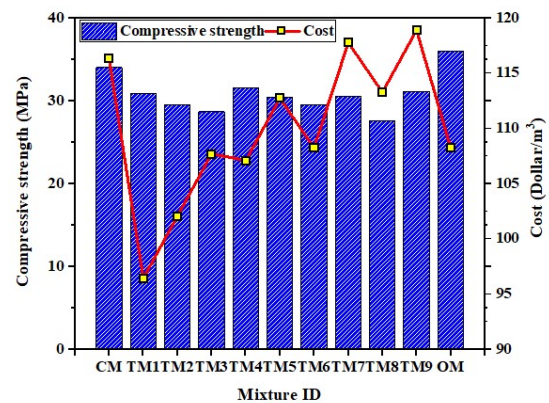


FIGURE 20. The correlation between mortar strength and production cost of synthetic aggregates.

5.2. Environmental factors analysis

To evaluate the environmental factor analysis of incorporating GGBFS and other binders into the production of synthetic aggregates, the emissions of CO₂, consumption of energy, and raw material ratio (RMR) were preferred. Table 9 provides a summary of the emissions of CO₂ and consumption of energy of all binders used in this study, as indicated in (59-62).

The ratio of raw materials is computed using Equation [9]:

$$RMR = \frac{m_t - m_g}{m_t} \times 100\% \quad [9]$$

Where m_t is the total weight of raw materials in the proportion of the mortar mixture and m_g is the weight of GGBFS.

TABLE 8. Cost of various raw materials used.

	Cement	GGBFS	MK	LP	Fine aggregate	Water	PPF	SP
Cost (Dollar/ton)	92.25	54.62	84.97	54.62	22.51	0.20	2120.97	2000

TABLE 9. Carbon dioxide emissions and consumption of energy by various binders.

	Cement	GGBFS	MK	LP	Fine aggregate	Water	PPF	SP
CO ₂ (kg/ton)	930	67	175	75	5	1	1710	600
Consumption of energy (MJ/0.1 m ³)	5.5	1.3	2.2	1	0.083	0.01	101	11.47

Figure 21 depicts the correlation between carbon dioxide emissions and environmental sustainability factors such as energy usage and ratio of raw materials. The unit of energy consumption was adopted as MJ/0.1 m³ to display the three parameters in a logical manner on the same graph. Typically, as the dosage of cement lowers and the GGBFS dosage rises, environmental sustainability parameters were declined. As expected, RMR is directly related to GGBFS dose, with the lowest raw material ratio identified in OM at 90.16 %. Even though TM1, TM2, TM3, and TM6 have the lowest carbon dioxide emissions and energy consumption among the nine mixtures, their compressive strength is the less preferred. The maximum reductions in carbon dioxide (CO₂) emissions, consumption of energy, and RMR were 44.50 %, 30.74 %, and 9.8 %, respectively, for optimized mixture.

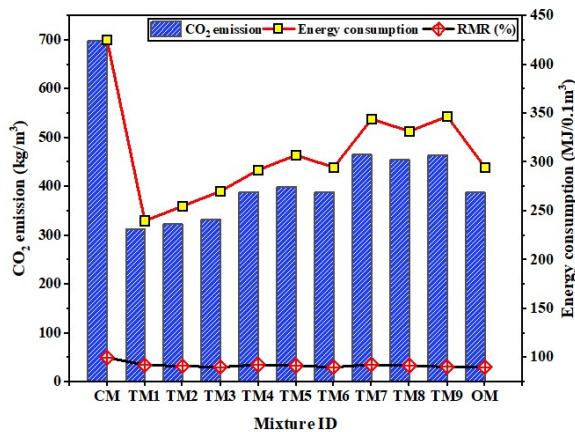


FIGURE 21. The correlation between CO₂ emissions and environmental sustainability parameters.

6. CONCLUSION

In the present research work, the feasibility of producing synthetic aggregate from industrial by-products has been investigated. This experiment involved optimizing the mix proportion, evaluating basic aggregate properties and microstructural investigation. The important findings of this study were summarized based on the laboratory-scale production of synthetic aggregates and microstructural analysis.

1. Synthetic aggregates containing industrial by-products as binders were produced success-

fully, and aggregate samples satisfied technical requirements.

- An acceptable composition was obtained through Taguchi's experimental design technique. In this study, the optimal mixture composition of synthetic aggregate was determined. The optimized mix is 50% ordinary Portland Cement, 40% ground granulated blast furnace slag, 5% Metakaolin, and 5% lime powder, at water to binder ratio of 0.31. In particular, FISA with a fiber content of 0.3% of the total binder.
- Bulk density of synthetic aggregates got reduced due to the lower specific gravity of GGBFS content. Hence both manufactured synthetic aggregates have bulk densities less than the specified limit (1200 kg/m³) according to standard requirements of BS EN 13055-1:2002. Additionally, the water absorption of SA and FISA aggregates was below the normal absorption limit of 25%.
- Mechanical properties, including aggregate impact and crushing value of synthetic aggregates (SA and FISA), showed good results with optimum binder content and longer curing period due to the formation of a dense microstructure and other hydration products. Especially, FISAs were stronger than SAs due to the integration of fibers and the development of a solid matrix.
- The examination of the mineralogy reveals that Montmorillonite (Al₂H₂O₁₂Si₄), Anorthite (CaAl₂Si₂O₈), Calcium aluminosilicate (Ca₂Al₂SiO₇), Lawsonite (CaAl₂Si₂O₇(OH)₂·H₂O), Quartz (SiO₂) and Calcite (CaCO₃) are the major phases observed in the XRD patterns of produced synthetic aggregates made with quaternary binders. AFM studies proved the existence of various surface roughness parameters of produced FISA were enhanced in comparison to SA.
- The most significant reductions in carbon dioxide (CO₂) emissions, consumption of energy, and raw material ratio (RMR) of 44.50 %, 30.74 %, and 9.0 %, respectively, for synthetic aggregates manufactured with an optimum mix contribute significantly to environmental sustainability.

The production of synthetic aggregates through industrial byproducts is not only a viable alternative to the extraction of natural aggregates but also a sustainable approach for waste management and contributes to waste recycling.

ACKNOWLEDGEMENT

The authors would like to thank the Vellore Institute of Technology, Vellore for providing lab facilities and material characterization instrumental facilities used in this investigation. A word of special thanks goes to the Department of Structural and Geotechnical Engineering, School of Civil Engineering for their continuous support during the conduction of experiments.

AUTHOR CONTRIBUTIONS:

Conceptualization: A. Abdul Rahim. Data curation: R. Vignesh. Formal analysis: R. Vignesh. Investigation: A. Abdul Rahim. Methodology: R. Vignesh. Project administration: A. Abdul Rahim. Resources: R. Vignesh. Software: R. Vignesh. Supervision: A. Abdul Rahim. Validation: A. Abdul Rahim. Visualization: R. Vignesh. Writing, original draft: R. Vignesh. Writing, review & editing: A. Abdul Rahim.

LIST OF SYMBOLS AND ACRONYMS

OPC – Ordinary Portland cement; **GGBFS** – Ground granulated blast furnace slag; **MK**- Metakaolin; **LP** – Lime powder; **SP** – Superplasticizer; **PPF** – Polypropylene fibers; **W/B** – Water to binder ratio; **CM** – Control mixture; **OM** – Optimized mixture; **TM** – Trail mixture; **ACV** – Aggregate crushing value; **AIV** – Aggregate impact value; **AAV** – Aggregate abrasion value; **ASV** – Aggregate soundness value; **SEM** – Scanning electron microscope; **EDX** - Energy Dispersive X-ray spectroscopy; **XRD** – X-ray diffractometer; **FTIR** - Fourier Transform infrared spectroscopy; **TGA** - Thermo-gravimetric analysis; **AFM** – Atomic force microscopy; **NA** – Natural aggregates; **SA** – Synthetic aggregates; **FISA** – Fiber intruded synthetic aggregates; **RMR** – Raw material ratio.

REFERENCES

- Kisku, N.; Joshi, H.; Ansari, M.; Panda, S.K.; Nayak, S.; Dutta, S.C. (2017) A critical review and assessment for usage of recycled aggregate as sustainable construction material. *Constr. Build. Mater.* 131, 721–740. <https://doi.org/10.1016/j.conbuildmat.2016.11.029>.
- Chu, S.H.; Jiang, Y.; Kwan, A.K.H. (2019) Effect of rigid fibres on aggregate packing. *Constr. Build. Mater.* 224, 326–335. <https://doi.org/10.1016/j.conbuildmat.2019.07.072>.
- Tuan, B.L.A.; Hwang, C.L.; Lin, K.L.; Chen, Y.Y.; Young, M.P. (2013) Development of lightweight aggregate from sewage sludge and waste glass powder for concrete. *Constr. Build. Mater.* 47, 334–339. <https://doi.org/10.1016/j.conbuildmat.2013.05.039>.
- González-Corrochano, B.; Alonso-Azcárate, J.; Rodas, M.; Barrenechea, J.F.; Luque, F.J. (2011) Microstructure and mineralogy of lightweight aggregates manufactured from mining and industrial wastes. *Constr. Build. Mater.* 25 [8], 3591–3602. <https://doi.org/10.1016/j.conbuildmat.2011.03.053>.
- Muduli, R.; Mukharjee, B.B. (2020) Performance assessment of concrete incorporating recycled coarse aggregates and metakaolin: A systematic approach. *Constr. Build. Mater.* 233, 117223. <https://doi.org/10.1016/j.conbuildmat.2019.117223>.
- Tian, K.; Wang, Y.; Hong, S.; Zhang, J.; Hou, D.; Dong, B.; Xing, F. (2021) Alkali-activated artificial aggregates fabricated by red mud and fly ash: Performance and microstructure. *Constr. Build. Mater.* 281, 122552. <https://doi.org/10.1016/j.conbuildmat.2021.122552>.
- Rashad, A.M. (2018) Lightweight expanded clay aggregate as a building material – An overview. *Constr. Build. Mater.* 170, 757–775. <https://doi.org/10.1016/j.conbuildmat.2018.03.009>.
- Alqahtani, F.K.; Rashid, K.; Zafar, I.; Iqbal Khan, M. (2021) Assessment of morphological characteristics and physico-mechanical properties of geopolymer green foam lightweight aggregate formulated by microwave irradiation. *J. Build. Eng.* 35, 102081. <https://doi.org/10.1016/j.job.2020.102081>.
- Nadesan, M.S.; Dinakar, P. (2017) Structural concrete using sintered flyash lightweight aggregate: A review. *Constr. Build. Mater.* 154, 928–944. <https://doi.org/10.1016/j.conbuildmat.2017.08.005>.
- Zafar, I.; Rashid, K.; Ju, M. (2021) Synthesis and characterization of lightweight aggregates through geopolymerization and microwave irradiation curing. *J. Build. Eng.* 42, 102454. <https://doi.org/10.1016/j.job.2021.102454>.
- Pekgöz, M.; Tekin, İ. (2021) Microstructural investigation and strength properties of structural lightweight concrete produced with Zeolitic tuff aggregate. *J. Build. Eng.* 43, 102863. <https://doi.org/10.1016/j.job.2021.102863>.
- Narattha, C.; Chaipanich, A. (2018) Phase characterizations, physical properties and strength of environment-friendly cold-bonded fly ash lightweight aggregates. *J. Clean. Prod.* 171, 1094–1100. <https://doi.org/10.1016/j.jclepro.2017.09.259>.
- Rehman, M.U.; Rashid, K.; Haq, E. U.; Hussain, M.; Shehzad, N. (2020) Physico-mechanical performance and durability of artificial lightweight aggregates synthesized by cementing and geopolymerization. *Constr. Build. Mater.* 232, 117290. <https://doi.org/10.1016/j.conbuildmat.2019.117290>.
- Rehman, M.U.; Rashid, K.; Zafar, I.; Alqahtani, F.K.; Khan, M.I. (2020) Formulation and characterization of geopolymer and conventional lightweight green concrete by incorporating synthetic lightweight aggregate. *J. Build. Eng.* 31, 101363. <https://doi.org/10.1016/j.job.2020.101363>.
- Morsy, M.S.; Alsayed, S.H.; Salloum, Y.A. (2012) Development of eco-friendly binder using metakaolin-fly ash-lime-anhydrous gypsum. *Constr. Build. Mater.* 35, 772–777. <https://doi.org/10.1016/j.conbuildmat.2012.04.142>.
- Mabeyo, P.E.; Ibrahim, Y.S.; Gu, J. (2020) Effect of high metakaolin content on compressive and shear-bond strengths of oil well cement at 80 °C. *Constr. Build. Mater.* 240, 117962. <https://doi.org/10.1016/j.conbuildmat.2019.117962>.
- Kalaivani, M.; Shyamala, G.; Ramesh, S.; Angusenthil, K.; Jagadeesan, R. (2020) Performance evaluation of fly ash/slag based geopolymer concrete beams with addition of lime. *Mater. Today Proc.* 27 [1], 652–656. <https://doi.org/10.1016/j.matpr.2020.01.596>.
- González-Corrochano, B.; Alonso-Azcárate, J.; Rodas, M. (2009) Production of lightweight aggregates from mining and industrial wastes. *J. Environ. Manage.* 90 [8], 2801–2812. <https://doi.org/10.1016/j.jenvman.2009.03.009>.
- Rahim, A.; Sharma, U.K.; Murugesan, K.; Sharma, A.; Arora, P. (2013) Multi-response optimization of post-fire residual compressive strength of high performance concrete. *Constr. Build. Mater.* 38, 265–273. <https://doi.org/10.1016/j.conbuildmat.2012.08.048>.
- Sevinç, A.H.; Durgun, M.Y.; Eken, M. (2017) A Taguchi approach for investigating the engineering properties of concretes incorporating barite, colemanite, basaltic pumice and ground blast furnace slag. *Constr. Build. Mater.* 135, 343–351. <https://doi.org/10.1016/j.conbuildmat.2016.12.209>.
- Dave, S. V.; Bhogayata, A.; Arora, N.K. (2021) Mix design optimization for fresh, strength and durability properties of ambient cured alkali activated composite by Taguchi method. *Constr. Build. Mater.* 284, 122822. <https://doi.org/10.1016/j.conbuildmat.2021.122822>.
- Shivaprasad, K.N.; Das, B.B. (2018) Determination of optimized geopolymerization factors on the properties of pelletized fly ash aggregates. *Constr. Build. Mater.* 163, 428–437. <https://doi.org/10.1016/j.conbuildmat.2017.12.038>.

23. Panagiotopoulou, C.; Tsivilis, S.; Kakali, G. (2015) Application of the Taguchi approach for the composition optimization of alkali activated fly ash binders. *Constr. Build. Mater.* 91, 17–22. <https://doi.org/10.1016/j.conbuildmat.2015.05.005>.
24. Teimortashlu, E.; Dehestani, M.; Jalal, M. (2018) Application of Taguchi method for compressive strength optimization of tertiary blended self-compacting mortar. *Constr. Build. Mater.* 190, 1182–1191. <https://doi.org/10.1016/j.conbuildmat.2018.09.165>.
25. ASTM C150. (2001) Standard specification for Portland cement. Annual Book of ASTM Standards.
26. ASTM C989. (2005) Standard specification for ground granulated blast-furnace slag for use in concrete and mortars. ASTM Int. 2–6.
27. ASTM C 618. (2014) Standard specification for coal fly ash and raw or calcined natural pozzolan for use in concrete, ASTM Int. 1–5. <https://doi.org/10.1520/C0618>.
28. Belarmin Xavier, C.S.; Abdul Rahim, A. (2023) Optimization and characterization of the ternary blended iron rich natural binder concrete system. *Constr. Build. Mater.* 363, 129838. <https://doi.org/10.1016/j.conbuildmat.2022.129838>.
29. Guo, L.; Wang, W.; Zhong, L.; Guo, L.; Wang, L.; Wang, M.; Guo, Y.; Chen, P. (2022) Influence of composite admixtures on the freezing resistance and pore structure characteristics of cemented sand and gravel. *Mater. Construcc.* 72 [347], e290 <https://doi.org/10.3989/MC.2022.16021>.
30. Tan, Ö.; Zaimoglu, A.S. (2007) Optimization of compressive strength in admixture-reinforced cement-based grouts. *Mater. Construcc.* 57 [288], 91–98. <https://doi.org/10.3989/mc.2007.v57.i288.67>.
31. ASTM C305. (2011) Standard practice for mechanical mixing of hydraulic cement pastes and mortars of plastic consistency. ASTM Int. 1–3.
32. ASTM C330.(2009) Standard specification for lightweight aggregates for structural concrete. Annual book of ASTM Standards.
33. ASTM C127-15. (2015) Standard test method for relative density (specific gravity) and absorption of coarse aggregate. Annual Book of ASTM Standards.
34. BS 812-110. (1990) Testing aggregates. BS 812 Part 110.
35. IS 5640 (1970) Method of test for determining aggregate impact value of soft coarse aggregates.
36. BS 812-112. (1990) Testing aggregates. BS 812 Part 112.
37. IS 2386. (2016) Methods of test for aggregates for concrete, Part IV : mechanical properties. Bur. Indian Stand.
38. IS:2386. (1963) Methods of test for aggregates for concrete. Bur. Indian Stand. 5, 1–14.
39. ASTM C109/C109M-02. (2020) Standard test method for compressive strength of hydraulic cement mortars. ASTM Int. 04, 9.
40. Vignesh, R.; Abdul Rahim, A. (2022) Mechanical and microstructural properties of quaternary binder system containing OPC-GGBS-Metakaolin-Lime. *Mater. Today Proc.* 64 [2], 970-975. <https://doi.org/10.1016/j.matpr.2022.05.074>.
41. BS EN 13055-1(2002) Lightweight aggregates - Part 1: Lightweight aggregates for concrete, mortar and grout. European committee for standardization.
42. Cioffi, R.; Colangelo, F.; Montagnaro, F.; Santoro, L. (2011) Manufacture of artificial aggregate using MSWI bottom ash. *Waste Manag.* 31 [2], 281–288. <https://doi.org/10.1016/j.wasman.2010.05.020>.
43. Gesoğlu, M.; Güneysi, E.; Öz, H.Ö. (2012) Properties of lightweight aggregates produced with cold-bonding pelletization of fly ash and ground granulated blast furnace slag. *Mater. Struct. Constr.* 45, 1535–1546. <https://doi.org/10.1617/s11527-012-9855-9>.
44. Colangelo, F.; Messina, F.; Cioffi, R. (2015) Recycling of MSWI fly ash by means of cementitious double step cold bonding pelletization: Technological assessment for the production of lightweight artificial aggregates. *J. Hazard. Mater.* 299, 181–191. <https://doi.org/10.1016/j.jhazmat.2015.06.018>.
45. Bate, S.C.C. (1979) Guide for structural lightweight aggregate concrete: report of ACI committee 213. *Int. J. Cem. Compos. Light. Concr.* 1 [1], 5–6. [https://doi.org/10.1016/0262-5075\(79\)90004-6](https://doi.org/10.1016/0262-5075(79)90004-6).
46. Gunning, P.J.; Hills, C.D.; Carey, P.J. (2009) Production of lightweight aggregate from industrial waste and carbon dioxide. *Waste Manag.* 29 [10], 2722–2728. <https://doi.org/10.1016/j.wasman.2009.05.021>.
47. Shi, M.; Ling, T.C.; Gan, B.; Guo, M.Z. (2019) Turning concrete waste powder into carbonated artificial aggregates. *Constr. Build. Mater.* 199, 178–184. <https://doi.org/10.1016/j.conbuildmat.2018.12.021>.
48. Venkata Suresh, G.; Karthikeyan, J. (2016) Influence of chemical curing technique on the properties of fly ash aggregates prepared without conventional binders. *J. Struct. Eng.* 43, 381–389.
49. Gesoğlu, M.; Güneysi, E.; Mahmood, S.F.; Öz, H. Öznur, Mermerdaş, K. (2012) Recycling ground granulated blast furnace slag as cold bonded artificial aggregate partially used in self-compacting concrete. *J. Hazard. Mater.* 235–236, 352–358. <https://doi.org/10.1016/j.jhazmat.2012.08.013>.
50. Tang, P.; Xuan, D.; Cheng, H.W.; Poon, C.S.; Tsang, D.C.W. (2020) Use of CO₂ curing to enhance the properties of cold bonded lightweight aggregates (CBLAs) produced with concrete slurry waste (CSW) and fine incineration bottom ash (IBA). *J. Hazard. Mater.* 381, 120951. <https://doi.org/10.1016/j.jhazmat.2019.120951>.
51. Güneysi, E.; Gesoğlu, M.; Ghanim, H.; Ipek, S.; Taha, I. (2016) Influence of the artificial lightweight aggregate on fresh properties and compressive strength of the self-compacting mortars. *Constr. Build. Mater.* 116, 151–158. <https://doi.org/10.1016/j.conbuildmat.2016.04.140>.
52. Gesoğlu, M.; Özturan, T.; Güneysi, E. (2007) Effects of fly ash properties on characteristics of cold-bonded fly ash lightweight aggregates. *Constr. Build. Mater.* 21 [9], 1869–1878. <https://doi.org/10.1016/j.conbuildmat.2006.05.038>.
53. Alqahtani, F.K.; Ghataora, G.; Dirar, S.; Khan, M.I.; Zafar, I. (2018) Experimental study to investigate the engineering and durability performance of concrete using synthetic aggregates. *Constr. Build. Mater.* 173, 350–358. <https://doi.org/10.1016/j.conbuildmat.2018.04.018>.
54. Mo, K.H.; Ling, T.C.; Cheng, Q. (2021) Examining the influence of recycled concrete aggregate on the hardened properties of self-compacting concrete. *Waste Biomass Valoriz.* 12, 1133–1141. <https://doi.org/10.1007/s12649-020-01045-x>.
55. Shahane, H.A.; Patel, S. (2022) Influence of design parameters on engineering properties of angular shaped fly ash aggregates. *Constr. Build. Mater.* 327, 126914. <https://doi.org/10.1016/j.conbuildmat.2022.126914>.
56. Karthik, A.; Sudalaimani, K.; Vijayakumar, C.T.; Saravanakumar, S.S. (2019) Effect of bio-additives on physico-chemical properties of fly ash-ground granulated blast furnace slag based self cured geopolymer mortars. *J. Hazard. Mater.* 361, 56–63. <https://doi.org/10.1016/j.jhazmat.2018.08.078>.
57. Samad, S.; Shah, A. (2017) Role of binary cement including Supplementary Cementitious Material (SCM), in production of environmentally sustainable concrete: A critical review. *Int. J. Sustain. Built Environ.* 6, 663–674. <https://doi.org/10.1016/j.ijsbe.2017.07.003>.
58. Karthik, A.; Sudalaimani, K.; Vijaya Kumar, C.T.; (2017) Investigation on mechanical properties of fly ash-ground granulated blast furnace slag based self curing bio-geopolymer concrete. *Constr. Build. Mater.* 149, 338–349. <https://doi.org/10.1016/j.conbuildmat.2017.05.139>.
59. Meddah, M.S.; Ismail, M.A.; El-Gamal, S.; Fitriani, H. (2018) Performances evaluation of binary concrete designed with silica fume and metakaolin. *Constr. Build. Mater.* 166, 400–412. <https://doi.org/10.1016/j.conbuildmat.2018.01.138>.
60. Mukherjee, A.; Sumit; Deepmala; Dhiman, V.K.; Srivastava, P.; Kumar, A. (2021) Intellectual tool to compute embodied energy and carbon dioxide emission for building construction materials. *J. Phys. Conf. Ser.* 1950, 012025. <https://doi.org/10.1088/1742-6596/1950/1/012025>.
61. Yu, J.; Chen, Y.; Leung, C.K.Y. (2019) Mechanical performance of Strain-Hardening Cementitious Composites (SHCC) with hybrid polyvinyl alcohol and steel fibers. *Compos. Struct.* 226, 111198. <https://doi.org/10.1016/j.compstruct.2019.111198>.
62. Medjigbodo, G.; Rozière, E.; Charrier, K.; Izoret, L.; Loukili, A. (2018) Hydration, shrinkage, and durability of ternary binders containing Portland cement, limestone filler and metakaolin. *Constr. Build. Mater.* 183, 114–126. <https://doi.org/10.1016/j.conbuildmat.2018.06.138>